Editors' Suggestion | Featured in Physics

Microscopy of Cavity-Induced Density-Wave Ordering in Ultracold Gases

Tabea Bühler,* Aurélien Fabre,* Gaia Bolognini, Zeyang Xue, Timo Zwettler, Giulia Del Pace,‡ and Jean-Philippe Brantut†

Institute of Physics and Center for Quantum Science and Engineering, Ecole Polytechnique Fédérale de Lausanne, CH-1015 Lausanne, Switzerland

(Received 13 November 2025; accepted 13 February 2026; published 6 April 2026)

We demonstrate high-resolution *in situ* imaging of density-wave ordering induced by cavity-mediated interactions in a unitary Fermi gas. We observe long-range spatial correlations throughout the formation of density waves, both for adiabatic preparation and following a quench, with a pattern controlled by the cavity mode structure. Our single-shot microscopic images together with the real-time readout of the cavity photons provide access to atom-photon correlations. We use this capability to investigate order fluctuations as a function of time following a quench and to directly confirm the correspondence between optical and atomic observables. Our system opens rich perspectives, from local patterning to correlation measurements in long-range interacting quantum gases.

DOI: 10.1103/h3zm-rnnx

Introduction—Cavity quantum electrodynamics is one of the most powerful platforms for quantum simulation. Photon exchanges between atoms within the cavity mode produce a tunable long-range interaction, which can reach large strength, overcoming other energy scales such as the one given by temperature [1], kinetic energy [2,3], potential energy [4], atom-atom repulsion [5,6], or Fermi pressure [7,8] to yield a superradiant phase. Unique to this platform, photons leaking from the cavity provide real-time, weakly destructive information about the dynamics of the ordering process, allowing for detailed investigations of order formation and dynamics [9–13]. Superradiance is accompanied by spatial ordering of the atoms, which can be detected as Bragg peaks using standard time-of-flight images [2]. However, both the photons leaking from the cavity and the Bragg peaks represent global observables, incapable of directly revealing order *in situ*: the photon signal carries information integrated over the entire mode volume, and time of flight similarly extracts the cloud-averaged phase coherence between neighboring sites [14] without direct access to density correlations. Moreover, time of flight does not reveal spatial order in incoherent systems such as Mott insulators or thermal gases, and it has strong limitations for Fermi gases close to unitarity due to interactions during the cloud expansion. For these reasons, local imaging and addressing capabilities have been developed for cold atom experiments in optical lattices [15–18] with transformative impact, from the detection of nonlocal orders [19,20] to the engineering of complex potential landscapes [21]. These breakthroughs call for the development of similar techniques for high-resolution observation and addressing at the scale of the self-ordering patterns in cavity-quantum electrodynamics experiments.

The technical overhead of combining high-resolution imaging, quantum degenerate gases, and the cavity-QED infrastructure represents a considerable challenge. High-aperture optics and cavity QED have recently been combined for thermal atoms in optical tweezers applications [22–28]. Innovative systems combining imaging and cavities along a single optical axis have been demonstrated on thermal gases [29]. However, none of these setups so far produced an *in situ* image of cavity-induced density-wave order. In this Letter, we present direct single-shot *in situ* absorption imaging of density waves formed in a unitary Fermi gas with strong cavity-mediated interactions. Our system, outlined in Fig. 1(a), combines the real-time detection of cavity photons used in our previous works [8,13,30] with a high-numerical aperture (0.39) imaging system capable of resolving the density waves on individual *in situ* images.

Observation of cavity-induced density-waves—We investigate cavity-induced self-ordering using our setup featuring a unitary Fermi gas in a high-finesse optical cavity [31]. We illuminate the atoms with a side-pump laser, which is detuned by $-2\pi \times 47.690$ GHz from the atomic D_2 transition and red detuned by $\tilde{\Delta}_c \sim$ MHz from the dispersively shifted cavity resonance. For an applied pump potential V_0 exceeding a critical value V_{0c}, a macroscopic density wave emerges, as illustrated in Fig. 1(b). Its spatial structure is determined by the interference pattern between the pump and cavity modes, and its amplitude Θ serves as the order parameter for the phase transition [8].

*These authors contributed equally to this work.

†Contact author: jean-philippe.brantut@epfl.ch

‡Present address: Department of Physics and European Laboratory for Nonlinear Spectroscopy (LENS), University of Florence, 50019 Sesto Fiorentino, Italy.

 © 2026 American Physical Society

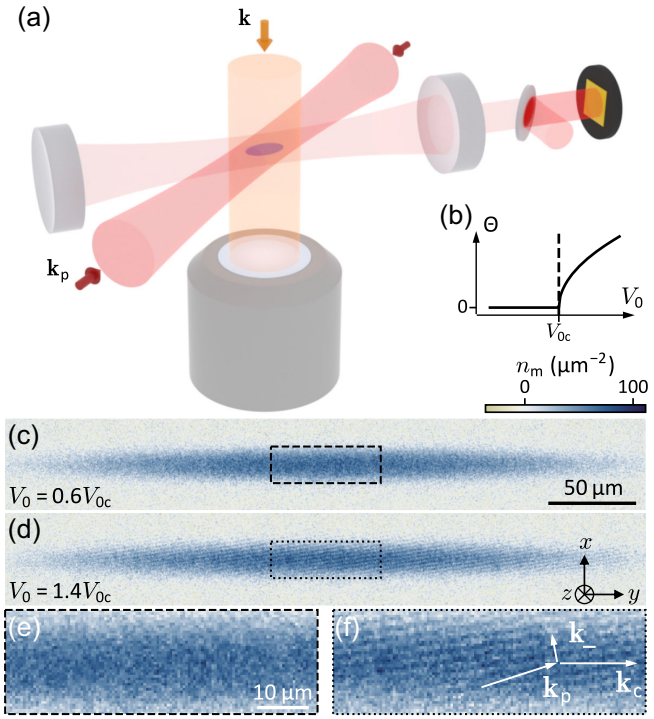


FIG. 1. Imaging of cavity-induced density waves. (a) Sketch of the experimental setup, with a unitary Fermi gas illuminated by a retroreflected side-pump beam with a wave vector $\mathbf{k}_\mathrm{p}$ (red). Light scattered by the atoms in the cavity mode (faint red) and leaking through the cavity mirrors is measured using heterodyne detection. A microscope objective oriented along the vertical direction collects absorption images of the atoms, using an imaging beam with wave vector $\mathbf{k}$ (light orange). (b) Schematic representation of the phase transition. Above a critical pump strength $V_{0\mathrm{c}}$, the system enters the ordered phase with a finite order parameter Θ. (c)–(f) Single shot absorption images of the atomic cloud for $V_0 = 0.6V_{0\mathrm{c}}$ (c) and $V_0 = 1.4V_{0\mathrm{c}}$ (d). (e),(f) Present magnified views on the image centers. In white, the wave vectors of the pump beam ($\mathbf{k}_\mathrm{p}$), the cavity field ($\mathbf{k}_\mathrm{c}$) and the resulting difference of the two ($\mathbf{k}_-$) are illustrated.

Our experiments start with a degenerate two-component unitary Fermi gas comprising typically $4.9(6) \times 10^5$ ^{6}Li atoms, at a temperature of $T/T_F \approx 0.16$, with a Fermi energy of $h \times 20(1)$ kHz, in the mode of a high-finesse optical cavity [32]. As it is sketched in Fig. 1(a), the pump beam is retroreflected and intersects the cavity at an angle of 18° [8,13]. Θ thus comprises two spatial frequency components $\mathbf{k}_-$ and $\mathbf{k}_+$ with periods of 2.14 μm and 0.34 μm, respectively. A commercial aspheric lens is used to image the $(\mathbf{k}_-, \mathbf{k}_+)$ plane using absorption imaging [33]. Critically, the numerical aperture of our lens yields a diffraction limit for coherent imaging of $\lambda_a/\mathrm{NA} = 1.7$ μm, λ_a being the wavelength of the imaging light, allowing us to resolve the long-wavelength component of the order parameter at $\mathbf{k}_-$. In addition, the cavity field leaking through one of the cavity mirrors is monitored using a heterodyne detection setup as sketched in Fig. 1(a) [33].

For a given realization of the experiment, we prepare the degenerate atomic gas and then increase adiabatically V_0 with a ramp rate of $\dot{V}_0 = 0.05 \times E_\mathrm{R}/\mathrm{ms}$, where E_R denotes the atomic recoil energy associated to $\mathbf{k}_\mathrm{p}$, the wave vector of the pump beam, $E_\mathrm{R} = \hbar^2\mathbf{k}_\mathrm{p}^2/2m = h \times 73.67$ kHz. Upon reaching a target value, we immediately take an absorption image with a measurement duration of 1 μs. As it is shown in Fig. 1, for low pump power (c), (e) the cloud has a Gaussian profile reflecting the underlying trap shape, while above $V_{0\mathrm{c}}$ (d),(f) the atomic density features a modulation at the wave vector $\mathbf{k}_-$, a direct manifestation of density-wave order. Since the imaging wavelength is larger than the modulation wavelength associated with $\mathbf{k}_+$, the high spatial-frequency component of the density cannot be observed by absorption imaging.

Image analysis and interpretation—To analyze the absorption images, we extract the measured column atomic density n_m following the technique of resonant, high-intensity absorption imaging [33–36], and evaluate the two-dimensional Fourier transform of the images $n_{\mathrm{m},\mathbf{k}}$. The modulus squared $|n_{\mathrm{m},\mathbf{k}}|^2$ is presented in Fig. 2(a), for $V_0 = 1.6(1)V_{0\mathrm{c}}$. Besides the peak around $\mathbf{k} = 0$, which reflects the envelope of the atomic cloud, it shows two sharp peaks at the $\pm\mathbf{k}_-$ points, corresponding to the density modulation visible in real space. Using an independent calibration of the magnification of the imaging system, we extract a period of 2.14(6) μm of the modulation, which is in agreement with the expected period along $\mathbf{k}_-$.

Quantitatively interpreting the modulation observed on the images requires understanding of coherent image formation for thick three-dimensional objects. Physically, the density-modulated cloud operates as a thick amplitude diffraction grating, where the first diffraction orders are captured by the imaging system and interfere with the zeroth order on the camera sensor to form the image. Because of the three-dimensional nature of the atomic cloud, the scattering efficiency into the first orders of diffraction is reduced for normal incidence of the imaging beam compared to incidence at the Bragg angle (see Ref. [33] for a quantitative discussion). To realize conditions in which imaging still reveals the density modulation, even for thick atomic clouds, images are taken with the imaging beam deviating from being orthogonal to $\mathbf{k}_-$ by an angle of $\alpha \approx 5.2(9)°$. In these conditions, we evaluate the suppression factor between the measured Fourier component at $\mathbf{k}_-$ and the actual Fourier component $n_{\mathrm{m},\mathbf{k}_-}/n_{\mathbf{k}_-}$ to be on the order of 0.24(8) [33]. The imaging of the envelope of the atomic cloud remains unaffected.

This effect prevents us from directly interpreting Fig. 2(a) as the spatial structure factor of the cloud. Nevertheless, in the immediate vicinity of $\mathbf{k}_-$, we can interpret $|n_{\mathrm{m},\mathbf{k}}|^2$ in terms of density correlations with a constant suppression factor [33]. Figure 2(b) shows cuts of Fig. 2(a) along x and y through the peak at $\mathbf{k}_-$, indicated with a dashed square,

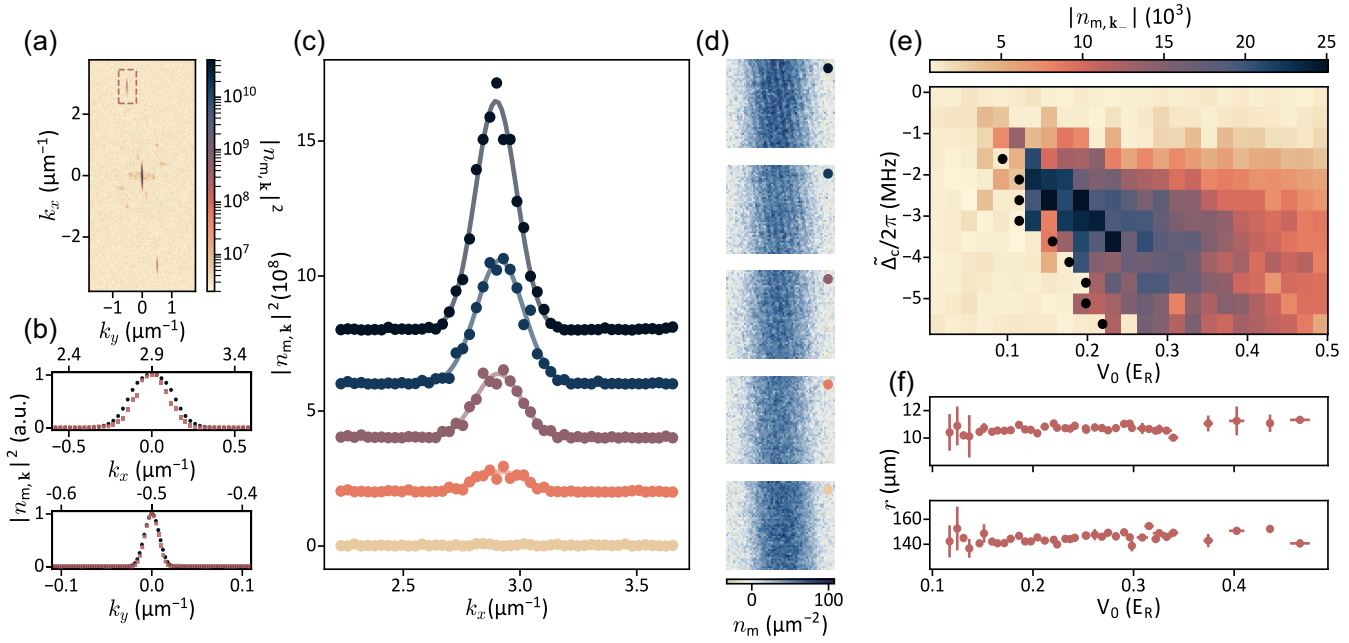


FIG. 2. Analysis of absorption pictures in Fourier space and imaging across the phase transition. (a) Modulus squared of Fourier transforms of measured atomic densities at an applied pump potential $V_0 = 1.6(1)V_{0c}$ (average over six repetitions). (b) Line cuts of (a) through the peak at $\mathbf{k}_-$, indicated with a dashed square, along the x direction (top) and the y direction (bottom) are shown as orange squares. As black circles line cuts of (a) at $\mathbf{k} = 0$ are shown for comparison. (c) Single-shot line cuts of $|n_{m,\mathbf{k}}|^2$ across the peak at $\mathbf{k}_-$ along x for $V_0 = 0.6, 1.3, 1.4, 1.5, 1.7V_{0c}$ (bottom to top, curves vertically offset by 2×10^8 for clarity). (d) Enlargement on the cloud centers of the corresponding absorption images in (c). (e) Fourier transform at $\mathbf{k}_-$ as a function of V_0 and $\tilde{\Delta}_c$. The black symbols represent the phase boundary extracted from the onset of the superradiant photon signal. (f) Correlation length of the density wave along the x (top) and y direction (bottom) as a function of V_0, above V_{0c} for $\tilde{\Delta}_c/2\pi = -2.6(2)$ MHz. The horizontal error bars represent the standard deviation of repeated measurements. The vertical error bars are obtained from a bootstrap resampling analysis.

together with the profile around $\mathbf{k} = 0$. Both profiles are normalized to one to cancel the suppression factor, making the shapes directly comparable. The two track each other closely, which is expected if the envelope of the density modulation follows the slowly varying density profile of the cloud. Our observations support the expectation that the density modulation has a single spatial frequency and is coherent over the entire atomic cloud. This is further confirmed by a local analysis of both Fourier amplitude and phase at $\mathbf{k}_-$, showing a uniform phase over the full extent of the atomic cloud [33].

Imaging across the transition—The Fourier spectrum around $\mathbf{k}_-$ allows us to track the density-wave order as it emerges above V_{0c}. Figure 2(c) presents cuts along the x direction of $|n_{m,\mathbf{k}}|^2$ through the peak at $\mathbf{k}_-$ as V_0 is increased across V_{0c}, showing the onset and growth of density-wave order. Enlargements of the center of the corresponding real-space images are shown in Fig. 2(d). Extracting the amplitude of the Fourier peak at $\mathbf{k}_-$ $|n_{m,\mathbf{k}}|$ via a Gaussian fit as a function of different system parameters allows to reconstruct the phase diagram in the $\tilde{\Delta}_c$-V_0 plane, as it is shown in Fig. 2(e), where V_0 is given in units of E_R. The phase boundary is faithfully reconstructed. Independently, we collect photons emerging from the cavity as V_0 is ramped up, allowing us to track the emergence of the density wave through its superradiant character, as it was done in all previous cavity-induced ordering experiments including our previous work [2,7,8]. The phase boundary extracted from the photon signal is indicated in Fig. 2(e) as black symbols (see Ref. [33] for more details) and is in good agreement with the one extracted from the absorption images.

The width of the peak at $\mathbf{k}_-$ in $|n_{m,\mathbf{k}}|^2$ can be interpreted as the inverse of the correlation length r of the density wave. We use a Gaussian fit to track r as V_0 is increased. The results are shown in Fig. 2(f) for extraction along the x and y directions, for $\tilde{\Delta}_c/2\pi = -2.6(2)$ MHz, showing almost no dependence on V_0. The extracted correlation lengths in the two directions differ by an order of magnitude, which reflects the aspect ratio of the atomic cloud. Closest to the critical point, error bars are dominated by shot-to-shot fluctuations of the exact threshold. However, for every data point showing a finite density-wave order the width of the Fourier peak is consistent with the width at higher V_0 within error bars. This demonstrates that the buildup of order occurs uniformly across the cloud, which is the expected behavior of ordering driven by infinite-range interactions [13,45] and is in agreement with the single-mode character of the cavity. It contrasts with order growing from local interactions, where a fluctuating

regime with limited spatial correlations is expected to exist in the vicinity of the transition [46].

Quench dynamics and correlations—In situ imaging provides access to density-density correlations in real space. The settings of cavity QED also provide real-time, weakly destructive information in the form of photons leaking continuously through the cavity mirrors. We now use this feature to investigate heterogeneous correlations between atomic and photonic observables, which underpin all the effective models of cavity-induced interactions [47]. For this, we perform an instantaneous quench into the ordered phase [12,13] and follow the buildup of order over an ensemble of realizations.

First, we observe $|n_{\mathrm{m},\mathbf{k}_-}|$ grow exponentially as the density wave instability builds up, and then saturate. As shown in previous works [12,13], the growth rate can span several orders of magnitude, controlled at a given detuning by the ratio V_0/V_{0c}. The ensemble average of $|n_{\mathrm{m},\mathbf{k}_-}|$ is shown as a function of time in Fig. 3(a) for $V_0 = 14.4(4)V_{0c}$. Its variance $\Delta|n_{\mathrm{m},\mathbf{k}_-}|^2$ increases and peaks as the system approaches the steady state, as shown in Fig. 3(b). Examples of images taken after 16 μs illustrate this variability [see Fig. 3(d)]. At longer time, order settles to a finite value and the variance is strongly reduced as the system reaches a steady state.

We leverage the intrinsic variability of $|n_{\mathrm{m},\mathbf{k}_-}|$ in the quench experiment to analyze correlations with the cavity photons. On the same ensemble of realizations, we evaluate the average of the cavity field amplitude $|a|$ and its variance $\Delta|a|^2$ as a function of time, as presented in the insets of Figs. 3(a) and 3(b). Similar to $\Delta|n_{\mathrm{m},\mathbf{k}_-}|^2$, the field variance peaks as the system approaches the steady state and then settles for longer times. Three examples of detected cavity field amplitudes are shown in Fig. 3(c) for the same experimental realizations as in Fig. 3(d). The extracted field endpoints are marked as square symbols and the orange line shows the applied V_0. We now evaluate density-field correlations over the full set of measurements. Figure 3(e) presents the correlation between $|n_{\mathrm{m},\mathbf{k}_-}|$ and the field amplitude $|a|$ from single realizations, in the early time following the quench. The field amplitude is normalized with the parameter $\eta_0 \propto \sqrt{V_0}$ [33]. The linear correlation is very strong down to the noise floor. A linear fit is shown as a black line.

The fluctuations observed in both $|n_{\mathrm{m},\mathbf{k}_-}|$ and $|a|$ are much larger than the underlying noise in the control parameters. They are expected from the initial quantum or thermal seed from which the density wave builds [45], or from dissipation leading to self-organized states with an incoherent mixture of cavity amplitudes [48]. Strong atom-field correlations are expected from the theory of cavity-mediated ordering: for large $\tilde{\Delta}_c$, the atomic and photonic degrees of freedom are adiabatically following each other, leading to the operator relation $\hat{a} = (\eta_0/\tilde{\Delta}_c)\hat{\Theta}$. This

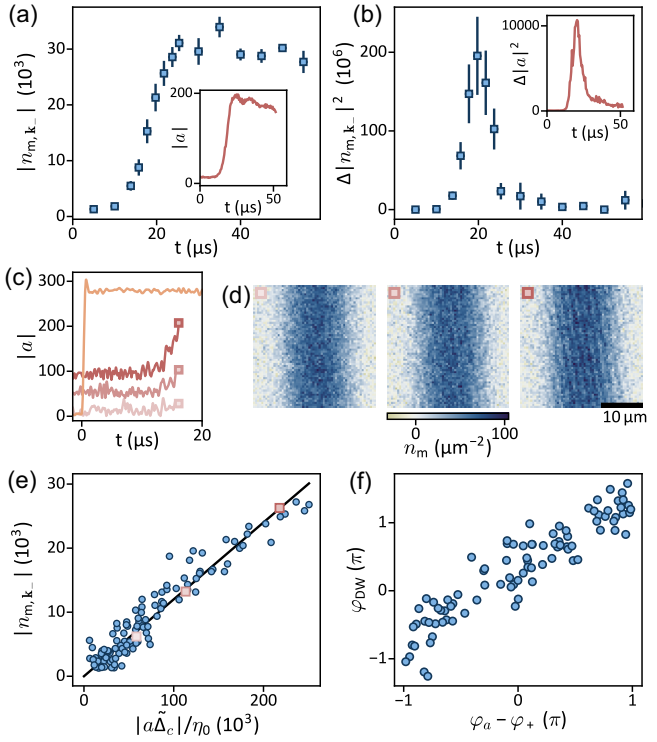


FIG. 3. Density-wave ordering after a quench. (a) Mean density modulation amplitude as a function of time, following a quench to $V_0 = 14.4(4)V_{0c}$. Inset: mean cavity field amplitude for the same realizations. The vertical error bars represent the standard deviation of repeated measurements. (b) Variance of the density modulation amplitude. Inset: variance of the cavity field amplitudes. The vertical error bars represent the statistical uncertainty due to finite sample size. (c) Cavity field amplitude for three experimental realizations at time $t = 16$ μs, (denoted by three different shades of pink) (offset for clarity). The extracted field endpoints are shown as a square symbols. The pump field is represented by the orange line. (d) Enlargement of absorption images recorded at the end of the three experimental realizations shown in (c). (e) Correlation between density-wave modulation and cavity field amplitude, each data point representing an individual experimental realization. The solid line represents a linear fit to the data. The realizations from panels (c),(d) are marked as square symbols. (f) Correlation between the phase of the density wave and the phase of the cavity field referenced to the phase of the pump field.

relation underlies the description of the system in terms of long-range interacting atoms and has, to our knowledge, never been tested experimentally. To highlight the general character of these correlations, we further confirmed them for quantum gases prepared away from unitarity [33]. Our observations of large and correlated fluctuations rule out a mean-field description of the atom-light system as a product state $\hat{\rho} = \hat{\rho}_{\mathrm{at}} \otimes |\alpha(t)\rangle\langle\alpha(t)|$ between an atomic state $\hat{\rho}_{\mathrm{at}}$ and a coherent state of the cavity field. Indeed, this would imply that the photon number follows Poisson statistics, i.e., that the variance and mean amplitudes would be proportional, in obvious contradiction with our

observations. Instead, our data can be described as an incoherent mixture of coherent states, each of them corresponding to a particular atomic configuration, as conjectured in [48,49].

In addition to the cavity field amplitude we measure the phase of the cavity field with respect to the pump beam $\varphi_a - \varphi_+$ [33]. Its counterpart on the images is the phase of the density modulation referenced to the position of the camera φ_{DW}, which can be extracted locally and over individual realizations. This information goes beyond the density correlations measured by the structure factor and can only be accessed by direct *in situ* observation. We evaluate phase correlations between the atomic density wave and the cavity field. The results are presented in Fig. 3(f). Because of the dependence of φ_{DW} on the phase of the pump field (see Ref. [33] for details), its measured values explore the full 2π range. The correlations between φ_{DW} and $\varphi_a - \varphi_+$, however, are again very strong, demonstrating the stability of the microscope setup throughout several experimental repetitions.

Density-wave ordering at higher-order modes—Our observation of a uniform phase of the density wave reflects the phase of the underlying fundamental transverse electromagnetic (TEM) cavity mode, TEM_{00}. If higher-order modes are involved in the ordering process, the density wave pattern within the atomic cloud can exhibit phase variations that cannot be retrieved by analyzing the overall phase of the emitted light. To demonstrate the ability to image inhomogeneous phase patterns, we reproduced the experiments with the pump laser frequency tuned to the close vicinity of the TEM_{01} cavity mode, located 2.634 (1) GHz away from the TEM_{00} mode. By monitoring the total number of photons leaking from the cavity, we observe the superradiant transition indicating density-wave ordering in this configuration. Exploiting the astigmatism of the cavity, which spectrally separates the two near-degenerate TEM_{01} and TEM_{10} modes [33], we target specifically the mode oriented orthogonal to the microscope axis and take images in the ordered phase. A sketch of the experiment is shown in Fig. 4(a), where the cavity field follows the shape of the TEM_{01} mode, whose electric field along the x direction is indicated in red. It has a nodal line as well as a π phase jump at the cavity axis. An example of an absorption image in this configuration is shown in Fig. 4(c), with an enlargement on the image center in Fig. 4(b). While the envelope of the density distribution is not affected by the change of the cavity mode, the density wave pattern exhibits a phase distortion at the center of the cloud, the location of the optical axis of the cavity. We analyze the recorded absorption images by computing $n_{m,\mathbf{k}_-}$ with a spatial resolution of 3.4 μm, allowing us to estimate both the amplitude and the phase of the density modulation locally. The results of the extracted amplitude and phase, averaged over 100 experimental repetitions, are shown in Fig. 4(d). A π phase shift between the two sides of

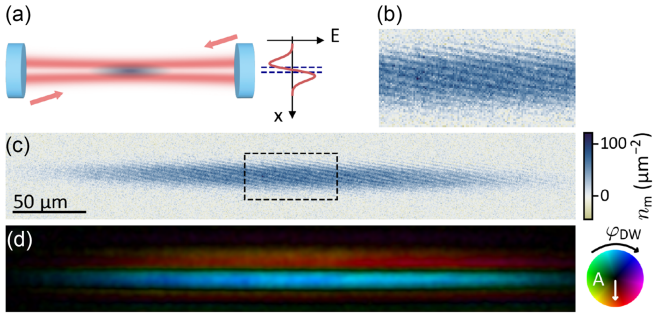


FIG. 4. Density-wave ordering at the first TEM cavity mode TEM_{01}. (a) Sketch of the experiment geometry with the transverse profile of the electric field amplitude of the TEM_{01} mode (red curve) and the full width at half maximum of the atomic density profile (dashed lines). (b) Enlargement of the center and (c) wide field image of the atomic density for density-wave ordering close to the first transverse mode of the cavity. (d) Local map of the amplitude (brightness) and phase (color map) of the density wave pattern across the cloud, averaged over 100 repetitions.

the cloud separated by a nodal line in the amplitude is clearly visible, matching the expected profile dictated by the TEM_{01} cavity mode.

Conclusion and outlook—We have demonstrated the direct observation of density-wave ordering in an ultracold Fermi gas using resonant absorption imaging, which enables the analysis of density correlations throughout the ordering process, as well as during ordering at higher-order cavity modes. The combination of single-shot imaging with single-trajectory readout of the cavity photons allowed us to reconstruct atom-field correlations, testing for the first time the foundations of cavity-induced interactions.

The ability to directly image the density-wave order opens a broad range of possibilities. First, it could be directly generalized to phase contrast imaging capable of observing magnetization patterns [50,51], which could emerge in the case of spin-imbalanced Fermi gases. In addition, imaging combined with radio-frequency spectroscopy [52] can be used to explore the fate of pairing in the presence of long-range interactions. This would be crucial when operating the experiment close to a photoassociation line, where the ordered phase acquires a pair-density wave character [30]. The microscope objective could also be used to project spatially engineered pump beams translating into complex, on-demand interaction patterns. Together with time-dependent manipulations, this can lead to effective finite-range interactions and new phases of matter [53,54].

Acknowledgments—We thank Kyuhwan Lee for careful reading of the manuscript and for discussions, Catalin-Mihai Halati for discussions, and Anastasiia Barysheva and Benedikt Röcken for their contributions to the characterization and mounting design of the imaging system. We acknowledge funding from the Swiss State Secretariat for Education, Research and Innovation

(Grants No. MB22.00063 and No. 20QU-1_215924) and the Swiss National Science Foundation (Grant No. 200020E_217124). A. F. acknowledges funding from the EPFL Center for Quantum Science and Engineering.

Data availability—The data that support the findings of this article are openly available [55].

[1] A. T. Black, H. W. Chan, and V. Vuletić, Observation of collective friction forces due to spatial self-organization of atoms: From Rayleigh to Bragg scattering, Phys. Rev. Lett. **91**, 203001 (2003).

[2] K. Baumann, C. Guerlin, F. Brennecke, and T. Esslinger, Dicke quantum phase transition with a superfluid gas in an optical cavity, Nature (London) **464**, 1301 (2010).

[3] J. Klinder, H. Keßler, M. Wolke, L. Mathey, and A. Hemmerich, Dynamical phase transition in the open Dicke model, Proc. Natl. Acad. Sci. U.S.A. **112**, 3290 (2015).

[4] J. Ho, Y.-H. Lu, T. Xiang, C. C. Rusconi, S. J. Masson, A. Asenjo-Garcia, Z. Yan, and D. M. Stamper-Kurn, Optomechanical self-organization in a mesoscopic atom array, Nat. Phys. **21**, 1071 (2025).

[5] J. Klinder, H. Keßler, M. R. Bakhtiari, M. Thorwart, and A. Hemmerich, Observation of a superradiant Mott insulator in the Dicke-Hubbard model, Phys. Rev. Lett. **115**, 230403 (2015).

[6] R. Landig, L. Hruby, N. Dogra, M. Landini, R. Mottl, T. Donner, and T. Esslinger, Quantum phases from competing short- and long-range interactions in an optical lattice, Nature (London) **532**, 476 (2016).

[7] X. Zhang, Y. Chen, Z. Wu, J. Wang, J. Fan, S. Deng, and H. Wu, Observation of a superradiant quantum phase transition in an intracavity degenerate fermi gas, Science **373**, 1359 (2021).

[8] V. Helson, T. Zwettler, F. Mivehvar, E. Colella, K. Roux, H. Konishi, H. Ritsch, and J.-P. Brantut, Density-wave ordering in a unitary fermi gas with photon-mediated interactions, Nature (London) **618**, 716 (2023).

[9] J. Léonard, A. Morales, P. Zupancic, T. Donner, and T. Esslinger, Monitoring and manipulating Higgs and goldstone modes in a supersolid quantum gas, Science **358**, 1415 (2017).

[10] N. Dogra, M. Landini, K. Kroeger, L. Hruby, T. Donner, and T. Esslinger, Dissipation-induced structural instability and chiral dynamics in a quantum gas, Science **366**, 1496 (2019).

[11] D. Dreon, A. Baumgärtner, X. Li, S. Hertlein, T. Esslinger, and T. Donner, Self-oscillating pump in a topological dissipative atom–cavity system, Nature (London) **608**, 494 (2022).

[12] Z. Wu, J. Fan, X. Zhang, J. Qi, and H. Wu, Signatures of prethermalization in a quenched cavity-mediated long-range interacting fermi gas, Phys. Rev. Lett. **131**, 243401 (2023).

[13] T. Zwettler, G. Del Pace, F. Marijanovic, S. Chattopadhyay, T. Bühler, C.-M. Halati, L. Skolc, L. Tolle, V. Helson, G. Bolognini, A. Fabre, S. Uchino, T. Giamarchi, E. Demler, and J. P. Brantut, Nonequilibrium dynamics of long-range interacting fermions, Phys. Rev. X **15**, 021089 (2025).

[14] F. Gerbier, A. Widera, S. Fölling, O. Mandel, T. Gericke, and I. Bloch, Interference pattern and visibility of a Mott insulator, Phys. Rev. A **72**, 053606 (2005).

[15] T. Gericke, P. Wurtz, D. Reitz, T. Langen, and H. Ott, High-resolution scanning electron microscopy of an ultracold quantum gas, Nat. Phys. **4**, 949 (2008).

[16] N. Gemelke, X. Zhang, C. Hung, and C. Chin, In situ observation of incompressible Mott-insulating domains in ultracold atomic gases, Nature (London) **460**, 995 (2009).

[17] W. S. Bakr, J. I. Gillen, A. Peng, S. Fölling, and M. Greiner, A quantum gas microscope for detecting single atoms in a Hubbard-regime optical lattice, Nature (London) **462**, 74 (2009).

[18] J. F. Sherson, C. Weitenberg, M. Endres, M. Cheneau, I. Bloch, and S. Kuhr, Single-atom-resolved fluorescence imaging of an atomic Mott insulator, Nature (London) **467**, 68 (2010).

[19] M. Endres, M. Cheneau, T. Fukuhara, C. Weitenberg, P. Schauß, C. Gross, L. Mazza, M. C. Bañuls, L. Pollet, I. Bloch, and S. Kuhr, Observation of correlated particle-hole pairs and string order in low-dimensional Mott insulators, Science **334**, 200 (2011).

[20] T. A. Hilker, G. Salomon, F. Grusdt, A. Omran, M. Boll, E. Demler, I. Bloch, and C. Gross, Revealing hidden antiferromagnetic correlations in doped Hubbard chains via string correlators, Science **357**, 484 (2017).

[21] P. M. Preiss, R. Ma, M. E. Tai, A. Lukin, M. Rispoli, P. Zupancic, Y. Lahini, R. Islam, and M. Greiner, Strongly correlated quantum walks in optical lattices, Science **347**, 1229 (2015).

[22] T. Đorđević, P. Samutpraphoot, P. L. Ocola, H. Bernien, B. Grinkemeyer, I. Dimitrova, V. Vuletić, and M. D. Lukin, Entanglement transport and a nanophotonic interface for atoms in optical tweezers, Science **373**, 1511 (2021).

[23] E. Uruñuela, M. Ammenwerth, P. Malik, L. Ahlheit, H. Pfeifer, W. Alt, and D. Meschede, Raman imaging of atoms inside a high-bandwidth cavity, Phys. Rev. A **105**, 043321 (2022).

[24] E. Deist, J. A. Gerber, Y.-H. Lu, J. Zeiher, and D. M. Stamper-Kurn, Superresolution microscopy of optical fields using tweezer-trapped single atoms, Phys. Rev. Lett. **128**, 083201 (2022).

[25] Y. Liu, Z. Wang, P. Yang, Q. Wang, Q. Fan, S. Guan, G. Li, P. Zhang, and T. Zhang, Realization of strong coupling between deterministic single-atom arrays and a high-finesse miniature optical cavity, Phys. Rev. Lett. **130**, 173601 (2023).

[26] X. Zhang, Z. Yu, H. Zhang, D. Xiang, and H. Zhang, Cavity dark mode mediated by atom array without atomic scattering loss, Phys. Rev. Res. **6**, L042026 (2024).

[27] L. Hartung, M. Seubert, S. Welte, E. Distante, and G. Rempe, A quantum-network register assembled with optical tweezers in an optical cavity, Science **385**, 179 (2024).

[28] B. Hu, J. Sinclair, E. Bytyqi, M. Chong, A. Rudelis, J. Ramette, Z. Vendeiro, and V. Vuletić, Site-selective cavity readout and classical error correction of a 5-bit atomic register, Phys. Rev. Lett. **134**, 120801 (2025).

[29] F. Orsi, N. Sauerwein, R. P. Bhatt, J. Faltinath, E. Fedotova, N. Reiter, T. Cantat-Moltrecht, and J.-P. Brantut, Cavity

microscope for micrometer-scale control of atom-photon interactions, PRX Quantum **5**, 040333 (2024).
[30] T. Zwettler, F. Marijanovic, T. Bühler, S. Chattopadhyay, G. Del Pace, L. Skolc, V. Helson, S. Uchino, E. Demler, and J.-P. Brantut, Cavity-mediated charge and pair-density waves in a unitary Fermi gas, Nat. Commun. **17**, 496 (2025).
[31] K. Roux, H. Konishi, V. Helson, and J.-P. Brantut, Strongly correlated fermions strongly coupled to light, Nat. Commun. **11**, 2974 (2020).
[32] T. Bühler, T. Zwettler, G. Bolognini, A. Fabre, V. Helson, G. Del Pace, and J.-P. Brantut, Direct production of fermionic superfluids in a cavity-enhanced optical dipole trap, SciPost Phys. **18**, 133 (2025).
[33] See Supplemental Material at http://link.aps.org/supplemental/10.1103/h3zm-rnnx for details on the experimental procedures, theoretical descriptions and supplementary data, which includes Refs. [34–44].
[34] G. Reinaudi, T. Lahaye, Z. Wang, and D. Guéry-Odelin, Strong saturation absorption imaging of dense clouds of ultracold atoms, Opt. Lett. **32**, 3143 (2007).
[35] M. Horikoshi, A. Ito, T. Ikemachi, Y. Aratake, M. Kuwata-Gonokami, and M. Koashi, Appropriate probe condition for absorption imaging of ultracold ^6Li atoms, J. Phys. Soc. Jpn. **86**, 104301 (2017).
[36] K. Hueck, N. Luick, L. Sobirey, J. Siegl, T. Lompe, H. Moritz, L. W. Clark, and C. Chin, Calibrating high intensity absorption imaging of ultracold atoms, Opt. Express **25**, 8670 (2017).
[37] K. Roux, V. Helson, H. Konishi, and J.-P. Brantut, Cavity-assisted preparation and detection of a unitary Fermi gas, New J. Phys. **23**, 043029 (2021).
[38] G. Birkl, M. Gatzke, I. H. Deutsch, S. L. Rolston, and W. D. Phillips, Bragg scattering from atoms in optical lattices, Phys. Rev. Lett. **75**, 2823 (1995).
[39] M. Weidemüller, A. Hemmerich, A. Görlitz, T. Esslinger, and T. W. Hänsch, Bragg diffraction in an atomic lattice bound by light, Phys. Rev. Lett. **75**, 4583 (1995).
[40] H. Miyake, G. A. Siviloglou, G. Puentes, D. E. Pritchard, W. Ketterle, and D. M. Weld, Bragg scattering as a probe of atomic wavefunctions and quantum phase transitions in optical lattices, Phys. Rev. Lett. **107**, 175302 (2011).
[41] R. A. Hart, P. M. Duarte, T.-L. Yang, X. Liu, T. Paiva, E. Khatami, R. T. Scalettar, N. Trivedi, D. A. Huse, and R. G. Hulet, Observation of antiferromagnetic correlations in the Hubbard model with ultracold atoms, Nature (London) **519**, 211 (2015).
[42] H.-J. Shao, Y.-X. Wang, D.-Z. Zhu, Y.-S. Zhu, H.-N. Sun, S.-Y. Chen, C. Zhang, Z.-J. Fan, Y. Deng, X.-C. Yao, Y.-A. Chen, and J.-W. Pan, Antiferromagnetic phase transition in a 3D fermionic Hubbard model, Nature (London) **632**, 267 (2024).
[43] J.-R. Li, J. Lee, W. Huang, S. Burchesky, B. Shteynas, F. Ç. Top, A. O. Jamison, and W. Ketterle, A stripe phase with supersolid properties in spin–orbit-coupled Bose–Einstein condensates, Nature (London) **543**, 91 (2017).
[44] V. Helson, T. Zwettler, K. Roux, H. Konishi, S. Uchino, and J.-P. Brantut, Optomechanical response of a strongly interacting fermi gas, Phys. Rev. Res. **4**, 033199 (2022).
[45] F. Marijanović, S. Chattopadhyay, L. Skolc, T. Zwettler, C.-M. Halati, S. B. Jäger, T. Giamarchi, J.-P. Brantut, and E. Demler, Dynamical instabilities of strongly interacting ultracold fermions in an optical cavity, arXiv:2406.13548.
[46] J. P. Sethna, *Statistical Mechanics: Entropy, Order Parameters, and Complexity*, Vol. 14 (Oxford University Press, New York, 2021).
[47] F. Mivehvar, F. Piazza, T. Donner, and H. Ritsch, Cavity qed with quantum gases: New paradigms in many-body physics, Adv. Phys. **70**, 1 (2021).
[48] C.-M. Halati, A. Sheikhan, H. Ritsch, and C. Kollath, Numerically exact treatment of many-body self-organization in a cavity, Phys. Rev. Lett. **125**, 093604 (2020).
[49] C.-M. Halati, A. Sheikhan, and C. Kollath, Theoretical methods to treat a single dissipative bosonic mode coupled globally to an interacting many-body system, Phys. Rev. Res. **2**, 043255 (2020).
[50] G. B. Partridge, W. Li, R. I. Kamar, Y.-a. Liao, and R. G. Hulet, Pairing and phase separation in a polarized fermi gas, Science **311**, 503 (2006).
[51] Y. Shin, M. W. Zwierlein, C. H. Schunck, A. Schirotzek, and W. Ketterle, Observation of phase separation in a strongly interacting imbalanced fermi gas, Phys. Rev. Lett. **97**, 030401 (2006).
[52] Y. Shin, C. H. Schunck, A. Schirotzek, and W. Ketterle, Tomographic RF spectroscopy of a trapped fermi gas at unitarity, Phys. Rev. Lett. **99**, 090403 (2007).
[53] M. Bonifacio, F. Piazza, and T. Donner, Laser-painted cavity-mediated interactions in a quantum gas, PRX Quantum **5**, 040332 (2024).
[54] R. Baumgartner, P. Pelliconi, S. Bandyopadhyay, F. Orsi, N. Sauerwein, P. Hauke, J.-P. Brantut, and J. Sonner, Quantum simulation of the Sachdev-Ye-Kitaev model using time-dependent disorder in optical cavities, arXiv:2411.17802.
[55] 10.5281/zenodo.18225513.